

Submitted to ApJ part 1

The optical counterpart of an Ultra-luminous X-Ray Source in NGC 5204

Ji-Feng Liu, Joel N. Bregman and Patrick Seitzer

Astronomy Department, University of Michigan, MI 48109

ABSTRACT

Ultra-luminous X-Ray sources are extra-nuclear point sources in external galaxies with $L_X = 10^{39}\text{--}10^{41}$ erg/s and are among the most poorly understood X-ray sources. To help understand their nature, we are trying to identify their optical counterparts by combining images from the Hubble Space Telescope and the Chandra Observatory. Here we report upon the optical counterpart for the ULX in NGC 5204, which has average X-ray luminosity of $\sim 3 \times 10^{39}$ erg/s and has varied by a factor of 50% over the last 10 years. A unique optical counterpart to this ULX is found by carefully comparing the Chandra ACIS images and HST WFPC2 and ACS/HRC images. The spectral energy distribution and the HST/STIS FUV spectrum of this object show that it is a B0 Ib supergiant star with peculiarities, including the $\lambda 1240$ N V emission line that is uncommon in B stellar spectra but has been predicted for X-ray illuminated accretion disks and seen in some X-ray binaries. Study of its FUV spectrum leads to a binary model for this ULX in which the B0 Ib supergiant is overflowing its Roche Lobe and accreting onto the compact primary, probably a black hole. This picture predicts an orbital period of ~ 10 days for different black hole mass, which can be tested by future observations.

Subject headings: Galaxy: individual(NGC 5204) — X-rays: binaries

1. INTRODUCTION

X-ray observations have revealed two categories of accretion powered X-ray point sources: the stellar mass X-ray binaries and the X-ray emission from active galactic nuclei. The first class has a typical luminosity range of $10^{33}\text{--}10^{38}$ erg/sec, powered by accretion onto a compact object such as a white dwarf, a neutron star or a black hole in a binary system. The

second class usually has an X-ray luminosity of $> 10^{41}$ erg/sec, powered by accretion onto a central super-massive black hole of mass 10^6 – $10^9 M_\odot$. X-ray point sources with luminosities within the range of 10^{39} – 10^{41} have also been observed in some external galaxies, first by the Einstein X-ray satellite (cf. Fabbiano 1989), later on by the ROSAT and ASCA X-ray satellites (e.g., Colbert & Mushotzky, 1999; Roberts & Warwick, 2000; Mizuno et al., 1999), and now by the Chandra X-ray satellite (e.g., Zezas et al., 2002). Some of these objects are nuclear sources and may be low luminosity AGNs, but others are extra-nuclear sources and form a different class. This class of extra-nuclear luminous sources has several names, such as intermediate luminosity X-ray objects (IXOs) and Ultra-luminous X-ray sources, or ULXs, which we use in this paper.

The observed luminosities of ULXs, if the X-ray emission is isotropic, require accreting black holes of masses $> 10^3 M_\odot$ if emitting at the level of 10^{-2} of the Eddington luminosity. Such black holes, if they exist, are the missing links between stellar mass black holes and super-massive black holes in the nuclei of galaxies. This idea is consistent with the X-ray spectral analyses of some ULXs in nearby galaxies (e.g., Makishima et al. 2000). However, the formation of such massive black holes is not predicted by stellar evolution theory, and it is still in debate about the prospect to form such objects in dense star clusters. Alternatively, these sources may be stellar mass black holes or neutron stars whose emission is beamed mildly or relativistically, thereby representing micro-quasars (King et al. 2001; Georganopoulos et al. 2002). If the emission is beamed, the intrinsic luminosities become sub-Eddington, and there are known examples of beamed Galactic X-ray sources (c.f., Mirabel & Rodriguez 1999). It is also possible that the luminosities are truly super-Eddington, for example, obtainable from accretion disks with radiation-driven inhomogeneities (Begelman, 2002).

To identify the ULXs at other wavelengths such as optical will supply information that is helpful to uncover the nature of these objects. For example, Pakull & Mirioni (2002) observed a sample of ULXs with ground-based telescopes, and were able to associate a number of ULXs to emission nebulae with kinematic ages of some million years. For the ULX positions, they used those derived from ROSAT HRI observations, which usually have errors of $\sim 5''$. Such a position error corresponds to 250 pc at a distance of 10 Mpc, and makes it impossible to identify down to single sources. However, with the advent of Chandra X-ray satellite, identifications down to single sources become possible owing to the sub-arcsecond spatial resolution of Chandra observations. Some efforts have already made along this line of thoughts. For example, by comparing Chandra ACIS-S and HST/WFPC2 observations of the "Antennae" starburst galaxies, Zezas et al. (2002) found that 10 out of 14 ULXs are associated with stellar clusters, with offsets between the X-ray sources and the clusters less than $2''$. Wu et al. (2002) found that the ULX in edge-on spiral galaxy NGC4565 is associated with a stellar cluster on the outskirt of the bulge. Also, as part of our search for

optical counterparts of ULXs in nearby galaxies, we (Liu, Bregman & Seitzer, 2002) found for the ULX in M81 a unique optical counterpart that is an O8 star, which is probably accreting mass onto a black hole of $20 M_{\odot}$ via Roche lobe overflow.

In this paper we report on the optical counterpart for the ULX in NGC 5204. In the last 10 years this ULX was observed twice by ROSAT PSPC, twice by ROSAT HRI, and twice by Chandra ACIS, with an average $L_X \sim 3 \times 10^{39}$ erg/s and a variation of 50%. With positions from Chandra ACIS observations, Roberts et al. (2001) and Goad et al. (2002) identified this ULX with three adjacent objects on HST WFPC2 images, the brightest one of which they estimated to be a young cluster with a few thousand member stars. Our re-analysis of the same data sets show that the most likely optical counterpart should be the faintest of the three objects, which is confirmed by new HST/STIS and HST ACS/HRC data as a single B0 Ib star. In §2, we present the observations utilized, the data analysis procedures, and the results. We discuss the implications of its optical identification in §3. For the distance to NGC 5204, we use 4.3 Mpc (Tully 1992). At such a distance, 1 HRC pixel, i.e., $0''.027$ which provides critical sampling at 6300 \AA , corresponds to a physical scale of 0.6 parsecs.

2. OBSERVATIONS AND DATA ANALYSIS

2.1. Data processing

A central issue in comparing optical and X-ray imaging data is registering the X-ray positions on the optical images, which requires accurate astrometry for both images. Here we use Chandra observations for X-ray images and HST observations for optical images, because these two instruments have the best astrometric accuracy available.

Two archive Chandra ACIS observations (Observation ID 2028, observed on 2001 January 9; Observation ID 2029, observed on 2001 May 2) were used to obtain the X-ray position of the ULX. To detect all discrete sources, we employed the CIAO tool `Wavdetect` on ACIS-S chips, although any detection method would find nearly all the same sources. Detected in both observations are the ULX and a second source $\sim 20''$ away, which is designated as CXOU J132940.1+582454 following the Chandra source naming convention. Both sources were reported in Roberts et al. (2001). The average X-ray position of the ULX is R.A. = 13:29.38.62, Decl = 58:25:5.6; the positions in two observations differ by $0''.4$, within the typical R.M.S. of absolute ACIS positions ($0''.6$; Aldcroft et al. 2000).

NGC 5204 was observed with HST twice, the first time in May, 2001 by HST WFPC2 using filter F606W and F814W(I), as part of a different program. Cosmic rays were not

removed from the images since the observations were single exposures. Both the ULX and J132940.1+582454 fall on the WF2 chips of these WFPC2 observations. Iraf tasks `metric`/`invmetric`, which correct the geometric distortion introduced by the camera optics, were used to transform between WFPC2 image positions (X,Y) and celestial coordinates (RA,DEC). The final relative positions are accurate to better than 0''.005 for targets contained on one chip, and 0''.1 for targets on different chips. The absolute accuracy of the positions obtained from WFPC2 images is typically 0''.5 R.M.S. in each coordinate (HST data handbook).

NGC5204 was also observed with the ACS/HRC on board HST in November 2002 for our program. The HRC image has a better spatial resolution, with a pixel size of 0''.027 that samples the HST point spread function critically at 6300 Å. HRC images were obtained in two filters, F220W and F435W, and for the F220W image, we obtained several images in a small raster pattern to better sample the PSF. The exposures were processed with `multidrizzle`¹ to combine the dithered images and remove the cosmic rays. Both the ULX and J132940.1+582454 lie in the HRC chip, leading to an accurate relative astrometric solution.

Direct comparisons between ACIS images and HST WF2 and ACS/HRC images yield several candidates of optical counterpart to the ULX. Registering the nominal X-ray position of the ULX onto the WF2 imageis (Figure 1), one finds within the 1'' nominal error circle three objects, which were designated as HST-1, HST-2, and HST-3 by Goad et al. (2002). For HRC images (Figure 1), the nominal error circle includes HST-3 (which is designated as U1), while HST-1 and HST-2 (which breaks down to a chain of separate sources) are outside of this error circle. This indicates a pointing offset of $\sim 1''.5$ between WFPC2 and ACS observations.

To find a unique optical counterpart to the ULX, we improved the positional accuracy further by relative astrometry between the ULX and J132940.1+582454, which fall on the same ACIS-S chip, the same WF2 chip, and the same ACS/HRC chip. Inspections of the WF2 images show that there is a source falling within the 1'' error circle of the nominal J132940.1+582454 position (Figure 2). On the HRC images, this same source falls within the 0''.6 error circle of the nominal J132940.1+582454 position. This source is a point source on HRC images; its non-pointlike appearance in the F606W image may be due to cosmic rays. This source is blue, with magnitudes listed in Table 2, and has a similar color as U1. Given its magnitude, it can not be an O/B star within our Galaxy, but it can be an O/B star in a high mass X-ray binary (HMXB) system in NGC 5204, or a background AGN.

¹see <http://stsdas.stsci.edu/pydrizzle/multidrizzle/>

In both cases, it could be a strong X-ray emitter. We believe it is the optical counterpart to J132940.1+582454, considering the low surface density of objects with similar brightness or brighter in its vicinity, which leads to a small chance (less than 1%) for it to be a random object falling into the error circle of J132940.1+582454. Given the WF2 position and HRC position of this optical counterpart to J132940.1+582454, and the X-ray position of J132940.1+582454, the ULX positions on WF2 images and HRC images were derived from its X-ray position (Table 1). The position error mainly comes from the centroiding error of J132940.1+582454. For the separation between the ULX and J132940.1+582454, the ACIS plate scale variation produces an error of $0''.02$. The rotation R.M.S. for both WFPC2 and ACIS-S chips are $\sim 0''.01$, and the error introduced by this effect is negligible. The final position error is $\Delta\alpha = 0''.25$, $\Delta\delta = 0''.16$.

2.2. Analysis of the Images

The much reduced error circles were overlayed on the WF2 images and HRC images in search of the optical counterpart to the ULX (Figure 1). On the WFPC2 images, while there are three objects within the $1''$ nominal error circle, among which HST-1 is the brightest, HST-3 is the only object (partly) within the reduced error circle, suggesting HST-3 is the unique optical counterpart to the ULX. On the HRC images, at the corresponding position of HST-3 within the reduced error circle is a point-like source (U1). On the edge of the error circle is another source, designated as U2, which is much fainter than U1, and marginally discernible in the WF2 images. HST-1 is $\sim 1''.5$ away from the reduced error circle; it does not even fall within the $1''$ nominal error circle like it does in the WF2 images.

The optical counterpart U1 is a point source instead of an extended source. On the F606W WF2 image, there is a spurious tail to the south-east of HST-3; however, this feature does not appear in the F814W WF2 image or the HRC images, and probably is a cosmetic feature due to cosmic rays. To study its spatial extent, we constructed the radial profiles for U1 as in the F220W and F435W HRC images (Figure 3). Its profiles are compared to the radial profiles for a nearby extended source, presumably a star cluster, and to a collection of 23 point-like sources in the proximity of the ULX. For the F220W HRC image, point-like objects have an average full-width at half measure (FWHM) of 3.40 ± 0.24 pixels, while U1 has a FWHM of 3.55 pixels, and the cluster has a FWHM of 5.68 pixels; for the F435W HRC image, point-like objects have an average FWHM of 2.47 ± 0.24 pixels, while U1 has a FWHM of 2.40 pixels, and the cluster has a FWHM of 4.02 pixels. On both images, the optical counterpart U1 is consistent with being a point source, and can be distinguished easily from an extended source.

HST-1 is a composite source as seen from the HRC images. Based on the HST WFPC2 observations, Goad et al. (2002) concluded that HST-1 is a young cluster composed of a few thousand stars. However, in the HRC images with higher spatial resolution, HST-1 can be decomposed into two components, one bluer component partly overlapping another redder component whose center is about 7 pixels (i.e., 4.2 parsecs) away. Such a decomposition is clearly shown in the contour plot (Figure 4) of the region around HST-1 and U1, which also shows that while the redder component is point-like, the bluer component shows complex infrastructures and is certainly not a single point source.

We can construct a spectral energy distribution (SED) from the four wide-band photometry measurements, i.e., ACS/HRC F220W (NUV), F435W, and WFPC2/WF2 F606W and F814W. For the ACS/HRC observations, aperture photometry was carried out with a 5 pixel annular aperture, and a 5% nominal error is adopted. For the WFPC2 observations, HSTphot (Dolphin 2000) was used to perform PSF fitting photometry to extract photon counts that are converted to STMAG. The results are listed in Table 2 for U1, U2, and HST-1, and the curves of the fluxes for the three objects are plotted in Figure 5. These curves show a trend of secular decline, reflecting the blackbody nature of the radiation. Note that the F606W and F814W fluxes, obtained from WF2 images, may contain contributions of nearby faint sources that can only be resolved in HRC images. The curve for HST-1 show a significant bump at redder wavelength as compared to the Rayleigh-Jeans extension of its NUV light. These extra light can be attributed to its redder component, while the NUV light can be mostly attributed to its bluer component.

The flux curves are compared to those of standard stars to shed light on the spectral types of these objects. These standard stars, whose absolute magnitudes and colors in the Johnson-Cousins system are taken from Schmidt-Kaler (1982), are placed at the distance to NGC 5204, and corrected for extinction toward U1 of $n_H = 10^{21} \text{ cm}^{-2}$ assuming Galactic relations $n_H = 5.8 \times 10^{21} E(B - V)$ (Bohlin et al. 1978) and $R_V = 3.1$. The adopted n_H value is inferred from the X-ray spectrum of the ULX, which can be fitted by an absorbed power law model with $n_H = 1.6 \pm 0.3 \times 10^{21} \text{ cm}^{-2}$ or an absorbed thermal bremsstrahlung model with $n_H = 5.4 \pm 1.7 \times 10^{20} \text{ cm}^{-2}$ (Roberts et al. 2001). The magnitudes and colors for U1 from the HRC and WFPC2 observations are consistent with those of stars of type O5 V, O7 III, or B0 Ib. The degeneracy of these different possibilities is lifted when the FUV spectrum of U1 is considered (see below). The fluxes from HST-1 are a few times brighter than U1 in the F220W band, making it impossible to be explained by a single O/B star. Combining with its complex non-pointlike infrastructures in the F220W band, we conclude the blue component of HST-1 is an OB association of at least a few O/B stars. The fluxes in the F606W and F814W bands, mostly from the red component, are more than 10 times higher than U1, and can be attributed to a young cluster of a few thousand stars (Goad et

al. 2002).

2.3. Spectral Analysis

To distinguish between O/B stars of different spectral types, MAMA/FUV spectral observations were taken by HST STIS in November, 2002 for our program. The placement of the $50'' \times 0''.2$ slit used in the observation is shown on the HRC images in Figure 1. The spectra of U1 and HST-1 were extracted and analyzed following standard procedures, and plotted in Figure 6. Galactic absorption lines such as $\lambda 1260$ and $\lambda 1527$ Si II lines can be seen in both spectra. These lines are usually rather narrow due to the low temperature of the absorbing medium; stellar lines are usually from high ionization levels and wider for the high stellar temperature.

As demonstrated in Figure 5, the U1 spectrum shows a spectral slope and flux level that are consistent with the wide-band photometry measurements. The STIS FUV spectrum of U1 was compared to the IUE stellar spectral library². The U1 spectrum declines steadily toward longer wavelength, and resembles the spectra of O stars and B stars earlier than B8. It is distinctly different from spectra of B8 and later stars which decline toward shorter wavelength.

More information can be obtained by comparing the spectral lines. The strongest line feature in the spectrum of U1 is the $\lambda 1299$ Si III line, which is commonly seen in hot O/B stars, confirming its identification as an O/B star. The equivalent width for this line is $\sim 1.5\text{\AA}$, which is suggestive of an O/B star cooler than about 25000 K (Prinja, 1990), so the most likely identification of U1 is a B0 Ib star rather than an O5 V star or an O7 III star. A low resolution model spectrum for a B0 I star from the Kurucz 1993 models³ is over-plotted in Figure 6 for comparison. Other line features implying an O/B star include the $\lambda 1175$ and $\lambda 1247$ C III lines, although these lines cannot be used to estimate the stellar temperature due to the high noise level.

The U1 spectrum shows some peculiarities for a B0 Ib star. The UV resonance lines of C IV $\lambda 1550$ and Si IV $\lambda 1400$, with P Cygni-type profiles indicative of high velocity hot O/B stellar winds, are commonly seen in B0 Ib stars and other O/B stars in the stellar spectral library. However, these conspicuous features are missing from the U1 spectrum. The $\lambda 1306$ emission line complex, a blend of O I and Si III lines commonly seen in optically thin HII

²<http://www-int.stsci.edu/jinger/iue.html>

³<ftp://ftp.stsci.edu/cdbs/cdbs2/grid/k93models/>

regions, is present in the U1 spectrum. However, this emission feature is usually not obvious in the spectra of O/B stars in the spectral library. It may be because these standard stars are all nearby Galactic stars, and a spectral observation includes only a small fraction of the H II regions surrounding the O/B stars. Another unusual feature is the high ionization $\lambda 1240$ N V emission line, which has an ionization energy (77.5 eV) above that of He II (54 eV). There is very little such ionizing radiation from a B0 star, and this line is not seen in normal B star spectra. The species N V can be achieved by collisional ionization at temperature $\sim 2 \times 10^5$ K, which does not occur in a B0 Ib star. One place to achieve such high ionization states is in an accretion disk and its corona, where the temperature can be higher than 10^7 K. Rather strong $\lambda 1240$ N V emission is predicted for an X-ray illuminated accretion disk and corona (Raymond, 1993), and it has been observed in low mass X-ray binaries (LMXBs) such as LMC X-3 (e.g., Cowley et al. 1994) and Hercules X-1 (e.g., Boroson et al. 2001).

In contrast, the HST-1 spectrum shows all the usual features of O/B stars, without the peculiarities. For example, the peculiar line features of $\lambda 1240$ N V and the $\lambda 1306$ emission line complex present in the U1 spectrum do not show up in the HST-1 spectrum. The $\lambda 1550$ C IV and the $\lambda 1400$ Si IV absorption line features typical of O/B stars are clearly present, revealing O/B stars in this composite source. This is consistent with our conclusion of HST-1 being an OB association plus a young cluster.

3. DISCUSSION

With improved astrometry, we found by combining Chandra ACIS data and HST WFPC2 and ACS/HRC data that the ULX in NGC 5204 has a unique optical counterpart U1. The spectral energy distribution of U1 shows it is an O5 V, O7 III or a B0 Ib star. With the help of its FUV spectrum, we found that U1 is a B0 Ib star with some peculiarities. For example, the resonance lines C IV $\lambda 1550$ and Si IV $\lambda 1400$ commonly seen in O/B stars due to hot O/B stellar winds are missing, while the $\lambda 1306$ emission line complex commonly seen in optically thin H II regions is present; the $\lambda 1240$ N V emission line is also present which indicates a temperature $\sim 2 \times 10^5$ K. All these observations can be explained by a binary model where the secondary of a B0 Ib supergiant is supplying fuel to the primary by Roche Lobe overflow. The observation of such a system supports the idea of King et al. (2001) that ULXs can be HMXBs with evolved secondary stars that overflow their Roche lobes.

The observed spectral features can easily fit into the proposed binary scenario. Due to the Roche potential, matter escaping the surface of the B0 Ib star flows rather smoothly along the equi-potential contours of the Roche Lobe, and accrete onto the compact primary

to form a disk. In the presence of an accretion disk and the large X-ray luminosity observed, Nitrogen in the disk/corona can be easily photoionized and/or collisionally ionized to N V, to give the N V $\lambda 1240$ emission line as observed in the spectrum of U1. The bulk of the matter does not escape to infinity, thus no large scale high velocity stellar wind is formed as in the cases of usual O/B stars. While there is a small amount of C IV $\lambda 1550$ and Si IV $\lambda 1400$ emission from the photosphere in the non local thermal equilibrium state, it is understandable that no significant such lines with P Cygni-type profiles emerge in the spectrum of U1 in the absence of large scale stellar winds. Another disadvantage against these lines is the presence of copious X-ray photons from the accretion disk, which may ionize Carbon and Silicon to ions higher than C IV and Si IV. The H II region around the binary system, with a size of ~ 10 parsecs at the distance of NGC 5204, can be included into the slit used in the observation. In this case, the strength of the $\lambda 1306$ emission line is larger than that of those standard O/B stars, in which the surrounding H II regions are only partially included.

This binary scenario is different from normal Galactic HMXBs, in which accretion is due to stellar wind capture. Galactic HMXBs typically have X-ray luminosities less than 10^{36} erg/s due to the low efficiency of stellar wind accretion. In this case strong beaming effects would be required to boost the luminosity above 10^{39} erg/s, which usually leads to small duty cycles. This is not the case for the ULX in NGC 5204, for which all 6 X-ray observations in the past 10 years were above 10^{39} erg/s. In this binary scenario, matter accretes onto the primary by Roche Lobe overflow, which is more efficient than stellar wind accretion. Some Galactic LMXBs accrete by Roche Lobe overflow, and their X-ray luminosities can be as high as 10^{39} erg/s. This will reduce the beaming factor required, if required at all, and increase the duty cycle, thus helping to explain the X-ray observations.

The period for such a system can be predicted given the mass and radius of the secondary and the mass of the primary. The mass and radius of the secondary can be determined empirically from its MK spectral type, then the period will solely depend on the primary mass under the Roche lobe overflow assumption. For the B0 Ib secondary, we take a mass of $25 M_{\odot}$ and a radius of $30 R_{\odot}$ (these are values for B0 Iab taken from Schmidt-Kaler 1982). The binary system would have a period of $\sim 204/290/295/284$ hours for a primary of mass $3/50/100/1000 M_{\odot}$ (Liu et al. 2002). Long term monitoring of this object may lead to a mass estimate and help to settle the debate whether the primary is a black hole of mass 10^3 – $10^4 M_{\odot}$ or a stellar mass black hole.

We are grateful for the service of HST and Chandra Data Archives. We would like to thank the anonymous referee for his helpful comments, and Charles Cowley, Ulisse Munari, Richard Gray, Joseph Cassinelli, Jimmy Irwin, Renato Dupke, and Eric Miller for helpful

discussions. We gratefully acknowledge support for this work from NASA under grants HST-GO-09073.

REFERENCES

Aldcroft, T.L., Karovska, M., Cresitello-Dittmar, M.L., Cameron, R.A., and Markevitch, M.L., 2000, Proc. SPIE, 4012, 650

Begelman, M.C., 2002, ApJ, 568, L97

Bohlin, R., Savage, B. D. & Drake, J. F., 1978, ApJ, 224, 132

Boroson, B., Kallman, T., and Vrtilek, S., 2001, ApJ, 562, 925

Colbert, E.J.M. and Mushotzky, R.F., 1999, ApJ, 519, 89

Cowley, A., Schmidtke, P., Hutchings, J., and Crampton, D., 1994, ApJ, 429, 826

Dolphin, A.E., 2000, PASP, 112, 1383

Fabbiano, G. 1989, ARA&A, 27, 87

Georganopoulos, M., Aharonian, F.A., and Kirk, J.G., 2002, å, 388, L25

Goad, M.R., Roberts, T.P., Knigge, C., and Lira, P. 2002, MNRAS, 335, L67

King, A.R., Davies, M.B., Ward, M.J., Fabbiano, G., and Elvis, M. 2001, ApJ, 552, L109

Liu, Ji-Feng, Bregmman, J.N., and Seitzer, P. 2002, ApJL, 580, L31

Makishima, K., Kubota, A., Muzuno, T., Ohnishi, T., Tashiro, M., et al. 2000, ApJ, 535, 632

Mirabel, I. F. and Rodriguez, L.F., 1999, ARA&A, 37, 409

Mizuno, T., Ohnishi, T., Kubota, A., Makishima, K., and Tashiro, M., 1999, PASJ, 51, 663

Pakull, M.W. and Mirioni, L., 2002, astro-ph/0202488

Prinja, R.K., 1990, MNRAS, 246, 392

Raymond, J., 1993, ApJ, 412, 267

Roberts, T. P. and Warwick, R. S. 2000, MNRAS, 315, 98 (RW2000)

Roberts, T. P., Goad, M. R., Ward, M. J., Warwick, R. S., et al. 2001, MNRAS, 325, 7

Goad, M. R., Roberts, T. P., Knigge, C., Lira, P. 2002, MNRAS, 335, 67

Schmidt-Kaler, Th., 1982, *Landolt-Bornstein: Numerical Data and Functional Relationships in Science and Technology*, eds. Schaifers, K. and Voigt, H.H., VI/2b, P.15-31

Tully R.B., Shaya E.J., Pierce M.J., 1992, ApJS, 80, 479

Vanbeveren, D., de Loore, C., and van Rensbergen 1998, A&ARev, 9, 63

Wu, H., Xue, S.J., Xia, X.Y., Deng, Z.G., and Mao, S.D. 2002, ApJ, 576, 738

Zezas, A., Fabbiano, G., Rots, A.H., and Murray, S.S. 2002, ApJ, 577, 710

Table 1. The optical counterpart to the ULX in NGC 5204

Object	ACIS-S3			WF2				HRC	
	RA	DEC	X	Y	RA	DEC	RA	DEC	
J132940.1+582454	13 29 40.19 $\pm 0.^{\prime\prime}24$	+58 24 53.9 $\pm 0.^{\prime\prime}16$	380.6	197.9	13 29 40.30	58 24 54.0	13 29 40.17	+58 24 54.3	
ULX	13 29 38.61 $\pm 0.^{\prime\prime}02$	+58 25 05.7 $\pm 0.^{\prime\prime}01$	272.9	332.2	13 29 38.72	58 25 05.8	13 29 38.58	+58 25 06.1	

Table 2. Photometric measurements for U1, U2, HST-1, and J132940.1+582454

Object	STMAG (mag)				F_{λ} (erg/s/cm ² /Å)			
	F220W	F435W	F606W	F814W	F220W	F435W	F606W	F814W
U1	19.99 ± 0.05	21.92 ± 0.05	22.97 ± 0.09	24.03 ± 0.08	3.664e-17	6.194e-18	2.362e-18	8.872e-19
U2	21.42 ± 0.05	23.67 ± 0.05	24.86 ± 0.08	25.72 ± 0.21	9.817e-18	1.236e-18	4.115e-19	1.872e-19
HST-1	19.18 ± 0.05	20.41 ± 0.05	20.63 ± 0.01	21.18 ± 0.01	7.727e-17	2.489e-17	2.025e-17	1.226e-17
J132940.1+582454	20.19 ± 0.05	21.77 ± 0.05	22.79 ± 0.09	23.81 ± 0.08	3.048e-17	7.112e-18	2.780e-18	1.086e-19

Note. — F_{λ} is related to STMAG by $F_{\lambda} = 10^{-0.4 \times (STMAG + 21.1)}$.

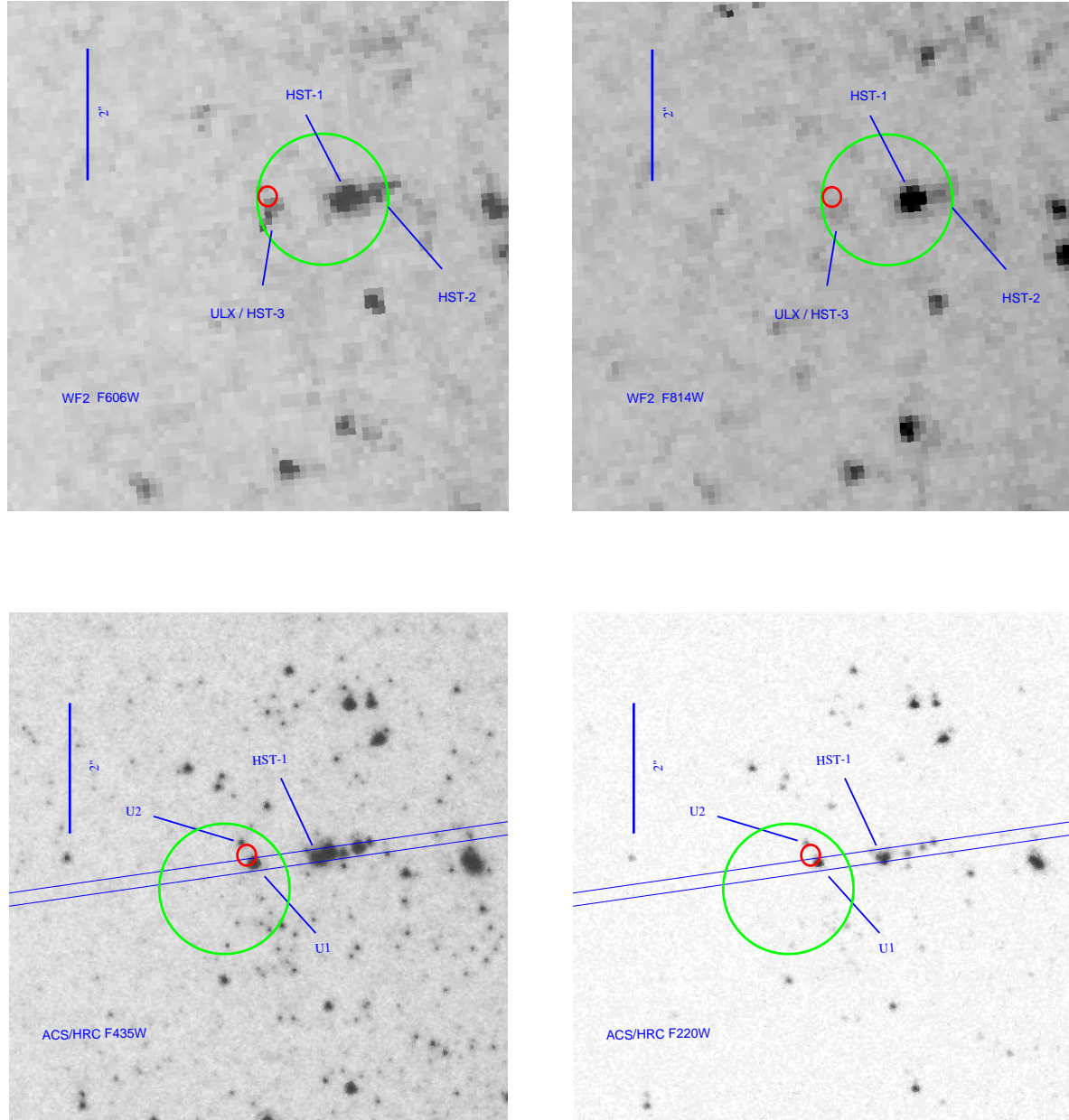


Fig. 1.— The optical counterpart to the ULX in NGC 5204. The small error ellipses, shown on the WF2 images and the HRC images, is described in the text. The 1'' error circle in the WF2 image around the nominal Chandra position was adopted by Goad et al.(2002); it includes different objects in the HRC images due to the pointing offsets between WFPC2 and ACS. The slit position for the STIS MAMA/FUV observation is shown in the HRC image.

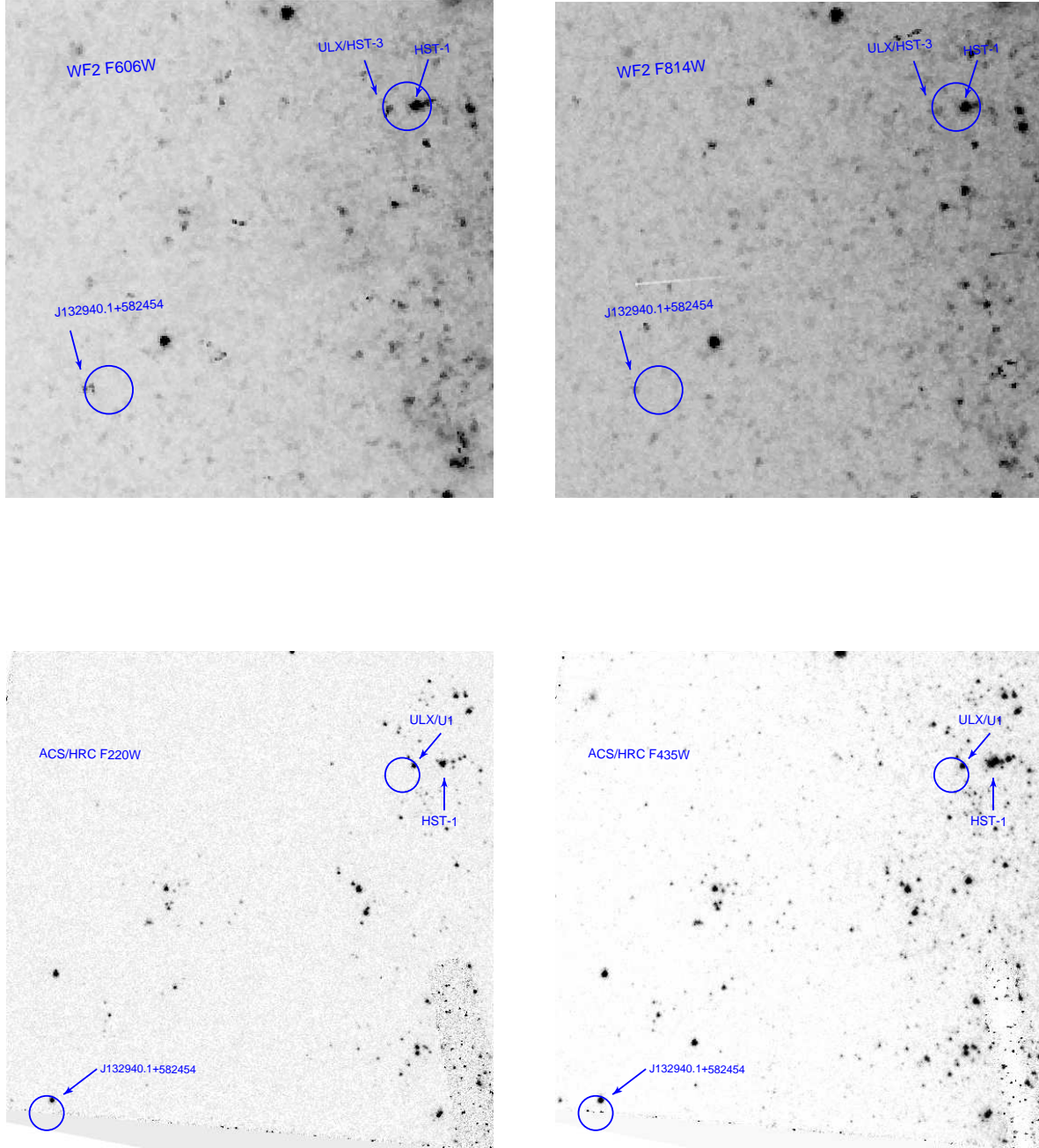


Fig. 2.— The optical counterparts to J132940.1+582454 and the ULX. stands for J132940.1+582454. The error circles on WF2 images have radii of $1''$, while the error circles on the HRC images have radii of $0''.6$.

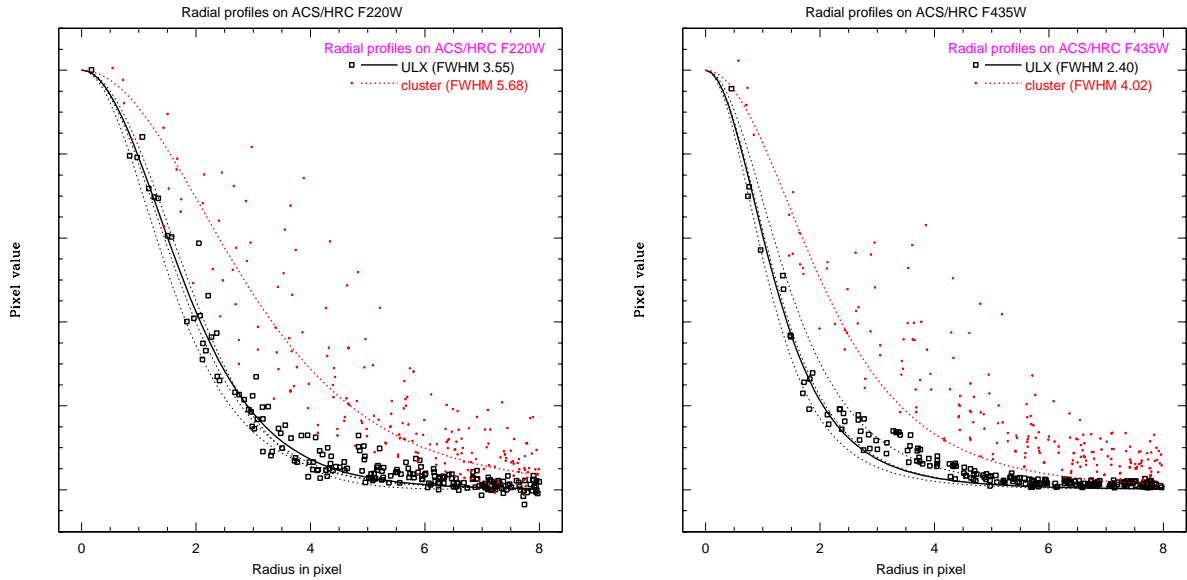


Fig. 3.— The radial profiles of U1 in HRC F220W and F435W CCD images. The squares and the thick solid line are the data and fit for the optical counterpart U1. Fits for some typical stellar profiles are plotted in thin dotted lines. For comparison radial profiles for a nearby cluster are plotted in thick dotted lines and crosses. In both images U1 is consistent with being a point source.

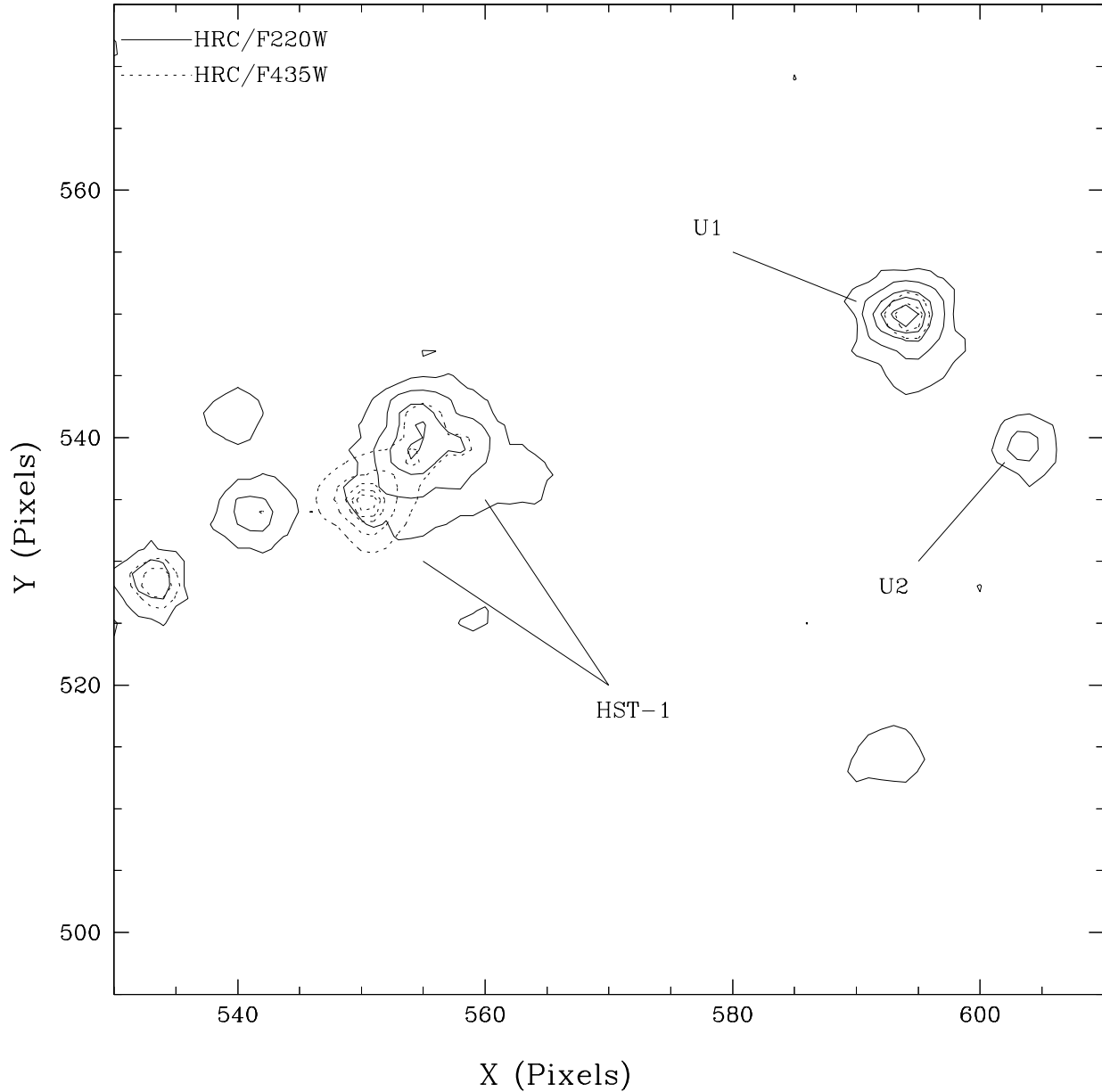


Fig. 4.— Contour plots for the HRC F220W and F435W images. A 80 pixel \times 80 pixel region including U1, U2 and HST-1 is shown. The optical counterpart U1 has a compact point-like core. HST-1, as one object in WF2 images, is now resolved into two components that are \sim 7 pixels apart.

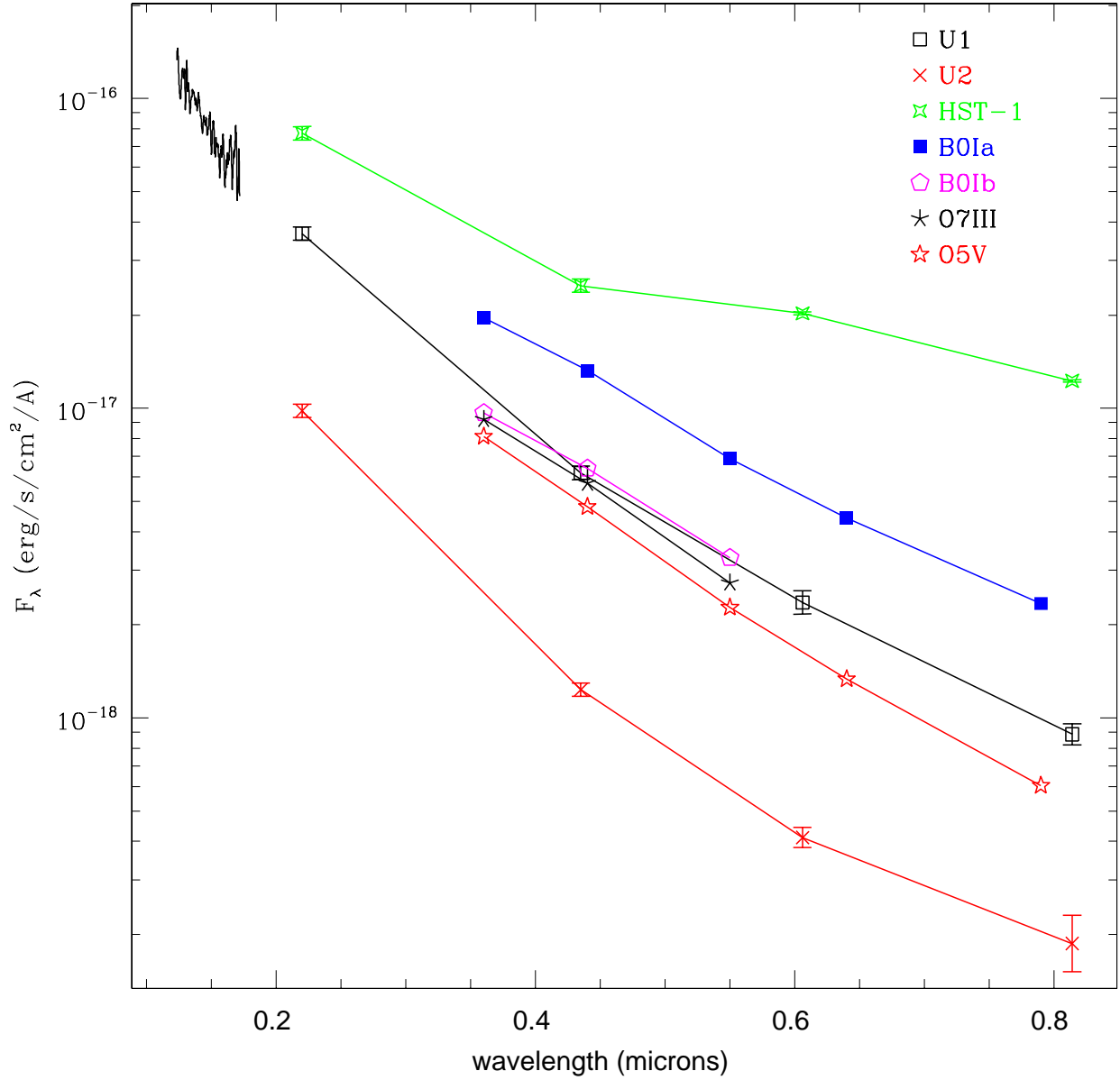


Fig. 5.— Wide-band photometry and FUV spectrum for the optical counterpart to the ULX in NGC 5204. Fluxes at 220Å, 435Å, 606Å, and 814Å for U1, U2 and HST-1 are plotted. For comparison are four standard stars placed with the ULX in NGC 5204 of types O5 V, O7 III, B0 Ia and B0 Ib, to which extinction inferred from X-ray absorption ($n_H = 10^{21} \text{ cm}^{-2}$, $R_V = 3.1$) is applied. The turn-up in the F606W and F814W fluxes of HST-1 is due to the red component of this composite source.

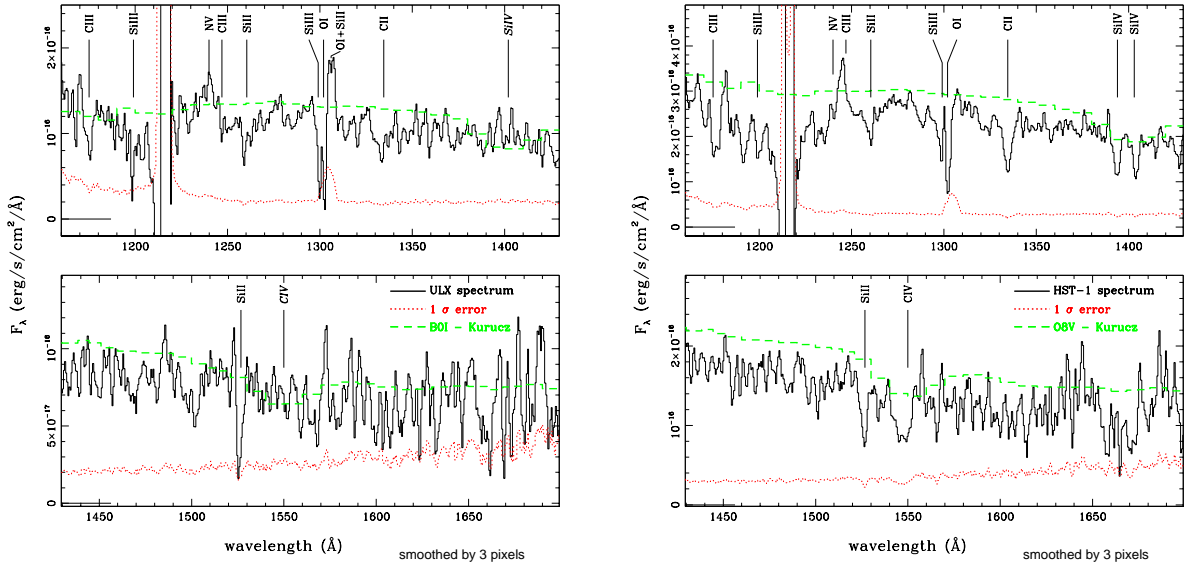


Fig. 6.— HST STIS MAMA/FUV spectra of U1 (left) and HST-1 (right). The 1σ error is plotted in dotted line. Low resolution model spectra from the Kurucz 1993 models are plotted in thick dashed lines for comparison. The O/B stellar features $\lambda 1550$ C IV and $\lambda 1402$ Si IV missing from U1 spectrum are labeled in italic.